Hydrographic and Current Measurements in the Area of the Angola–Benguela Front

H. U. LASS, M. SCHMIDT, V. MOHRHOLZ, AND G. NAUSCH

Institut für Ostseeforschung Warnemünde, Rostock-Warnemunde, Germany

(Manuscript received 29 March 1999, in final form 6 December 1999)

ABSTRACT

The structure and flow in the area of the Angola–Benguela front was studied under the auspices of BENEFIT (Benguela Environment–Fisheries Interaction and Training) during one of the starting cruises of the program with the R/V *P. Kottzov* from 20 April to 13 May 1997. The dataset acquired in the shelf area between 13°30′S and 17°S consists of CTD casts down to 1200 dbar, two sections of towed CTD, and seven tracks of towed acoustic Doppler current profiler measurements. Throughflow measurements of the temperature and salinity were performed continuously during the cruise. Daily National Aeronautics and Space Administration scatterometer (NSCAT) wind data with ½° resolution were analyzed for April and May 1997 in the area bounded by 5°N, 35°S and 10°W, 20°E.

The Angola–Benguela Front was observed at 16°30′S separating 40-m thick, tongue-shaped, warm and saline Angola Current water in the north from the cold and less-saline water of the Benguela in the south. In contrast to temperature, the pattern of salinity distribution in the tongue split northward into a northwestern and a coastal branch.

Strong downwelling was observed between 60- and 500-m depth on the shelf at 15° and 17°S. The core of the Antarctic Intermediate Water was found at a depth of 800 m throughout the whole region with a salinity of about 34.50 psu decreasing poleward.

A poleward current of 1 Sv entered the studied area through the northern boundary at 13°30′S. Additionally, an eastward directed geostrophic current of 6 Sv driven by the cyclonic wind stress curl entered the region from the northwest in the upper 400 m bending southward along the shelf edge at 15°S and exited the cruise area at 17°S as a coastal boundary current with a volume transport of about 7 Sv. The importance of this current as a link between the cyclonic gyre in the Angola Dome area and the source region of the Benguela Current is discussed.

1. Introduction

The Benguela is one of the four eastern boundary regimes of the World Ocean. Within the Benguela the northward flowing Benguela Current is the eastern boundary current of the South Atlantic subtropical gyre. See Peterson and Stramma (1991) for a review of the upper-level circulation in the South Atlantic. The prevailing winds in the coastal region off South West Africa (see Fig. 1) drive coastal upwelling of cold, nutrient-rich water associated with equatorward surface jets along the shelf-edge between Cape Point (34.35°S) and Cape Frio (18.4°S).

At the northern boundary of the Benguela the Angola–Benguela front (ABF) sharply separates the nutrient-poor warm Angola Current water from the nutrient-rich cold water of the Benguela and represents a transition zone between the more tropical ecosystem in the north and the upwelling-driven ecosystem in the south. The cold northward flowing shelf edge current of the Benguela and the warm southward propagating waters of the Angola Current confluence at about 15°S.

Circulation and dynamics of the Benguela are well known. See Nelson and Hutchings (1983), Shannon (1985), Shannon and Nelson (1996), and Chapmann and Shannon (1985) for a summary. The Angola Current and the Angola–Benguela front are not so well studied. A first description of both was given by Janke (1920) based on ship log data. Large-scale properties of the Angola Current have been derived from hydrographic data by Moroshkin et al. (1970) and Bubnov (1972). Near synoptic surveys of the Angola Current were performed by Diaz (1983a,b) revealing the vertical structure of Angola Current water.

Seasonal variations and mesoscale properties of the Angola–Benguela front have been derived from historic hydrographic data (Shannon et al. 1987), as well as from satellite based SST observations, Lutjeharms and Meeuwis (1987), Meeuwis and Lutjeharms (1990), and Kostianoy (1997). According to these observations the confluence zone is characterized by a permanent front with

Corresponding author address: H. U. Lass, Institut für Ostseeforschung Warnemünde, Seestr. 15, D-18119 Rostock-Warnemünde, Germany.
E-mail: lass@io-warnemuende.de

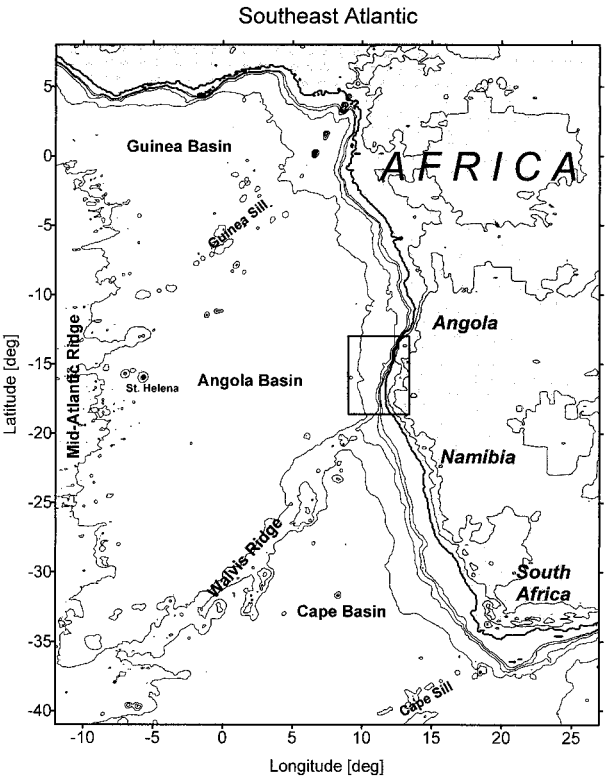

FIG. 1. Topography and coastal configuration of the SW Atlantic ocean. The square indicates the area of investigation during the cruise.

strong horizontal gradients in temperature as well as salinity in the upper 50 m. The front is aligned normal to the coast and its seaward extension varies between 200 and 600 km in austral fall. The average width of the front is about 200 km, but the actual width can be much smaller. Multiple sharp fronts can also occur. Interannual, seasonal as well as mesoscale feature, for example, eddies, meanders, and filaments cause great temporal and spatial variability in the frontal zone.

During southward intrusions of warm, saline surface waters onto the Namibian shelf the Angola–Benguela front is displaced to about 23°S (Shannon et al. 1986). These extreme events occur about once a decade in austral summer and are denoted as Benguela Niños.

The dynamics of the ABF is not well known. There are several assumptions on the most important processes maintaining the front. Shannon et al. (1987) assume that the Angola Dome may control the dynamics of the front. The Angola Dome is a cyclonic eddy doming of the thermocline at about 10°S, 9°E, which was first documented by Mazeika (1967). The dynamic topography and the geostrophic transport in the area of the dome was estimated by Gordon and Bosley (1991) as well as by Waconge and Piton (1992). They found an cyclonic gyre at 13°S, 10°E with the South Equatorial Current (SEC) west of the center, the eastward flowing South Equatorial Countercurrent (SECC) at the northern edge of the dome bending into the Angola Current on its eastern edge along the African coast, and a westward flowing current south of the dome. The transport around the gyre is about 5 Sv (Sv $\equiv 10^6$ m^3 s^{-1}). According to McClain and Firestone (1993), the Angola Dome is generated by a local maximum of Ekman suction. Yamagata and Iizuka (1995) could simulate seasonal variations of the Angola Dome with a numerical circulation model driven by climatological wind fields of Hellermann and Rosenstein (1983). In their model the cyclonic circulation around the Angola Dome links the SECC with the Angola Current and the SEC in the east, and south, and the SEC with SECC in the west and north. Fennel (1999) could show with an analytical model of the Benguela system, forced by longshore windstress of increasing strength in the offshore direction, that it responds with a poleward coastal current near the northern boundary.

The Benguela Niños are believed to be triggered by a relaxation of the equatorial winds in the western Atlantic (Shannon et al. 1986). This generates a free equatorial Kelvin wave propagating along the equatorial wave guide and continuing with poleward propagation along the west coast of Africa. Gammelsrod et al. (1998) found that the 1995 Benguela Niño was characterized by large-scale advection of near-equatorial surface water.

There is evidence that continental shelf waves propagate poleward along the coast of southwest Africa (Hagen 1981), governing structure, timescales, and propagation speeds of the mesoscale variability of the currents on the shelf.

2. Data sampling

CTD casts performed on a station grid shown in Fig. 2 have been combined with towed CTD, towed acoustic Doppler current profiler (ADCP), and underway measurements of wind velocity and sea surface temperature, as well as sea surface salinity, in order to resolve the horizontal pattern associated with the Angola–Benguela front area. The final configuration of the station grid was fixed during the cruise according to the actual position of the front derived from real time satellite images of the sea surface temperature (SST) provided generously by Scarla Weeks, University of Cape Town, and received on the vessel via INMARSAT B during the cruise.

Once a CTD section was completed the ADCP was towed along the same way back on starboard side simultaneously with the Scanfish towed on portside behind the ship. Towing speed varied between 3 and 3.5 m s^{-1}.

Vertical profiles of temperature, salinity, oxygen, fluorescence, and back-scattered light have been measured by a CTD SBE9+ on 68 stations. Water samples have been taken for chemical and biological analysis by a 12 51 bottle rosette sampler. The cast went down from

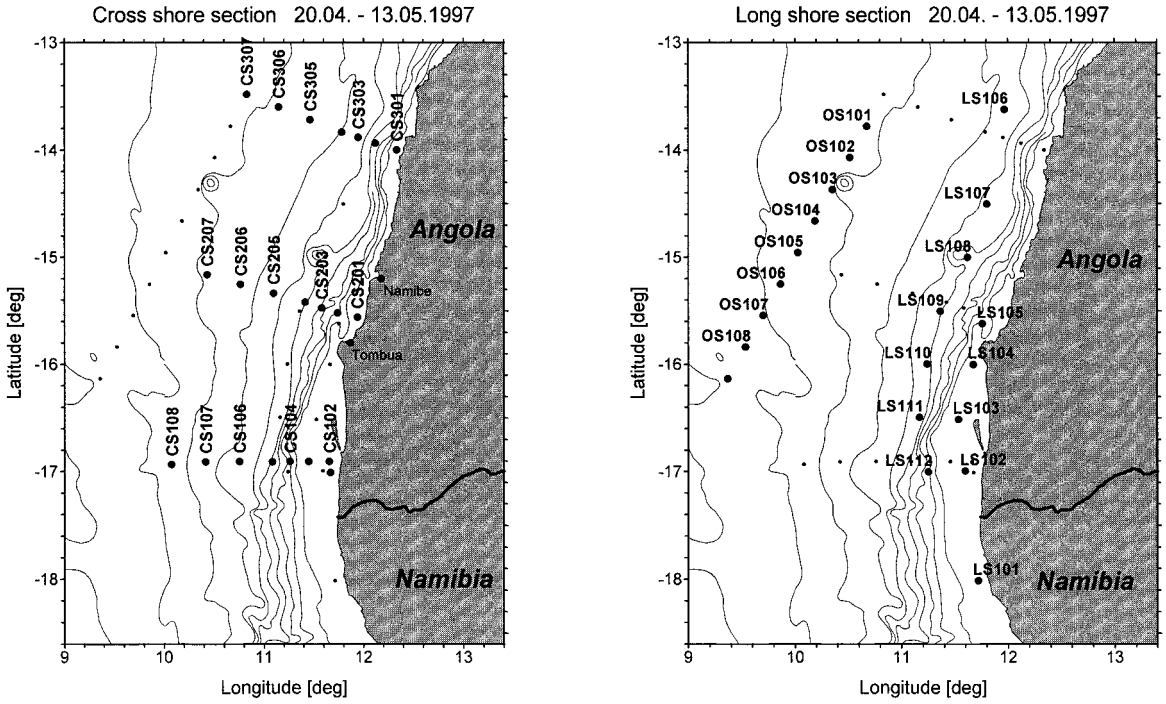

FIG. 2. Station grid of the R/V *P. Kottzov* cruise from 20 April to 12 May 1997.

the surface to 1200 dbar or near the bottom with a lowering speed of 0.5 m s^{-1} in the upper 150 m and 0.8 m s^{-1} below this depth.

Pre and post cruise calibrations of the CTD as well as comparison measurements during the cruise indicated that no corrections were necessary resulting in an standard error of 0.003 K and 0.003 psu for temperature and salinity, respectively. The pressure sensor was corrected with an offset of -0.50 dbar. The remaining standard error was 0.1 dbar.

The raw data of the CTD cast have been processed by Seabird post processing routines resulting in three profiles averaged in 1-, 5-, and 10-dbar bins.

Oxygen concentration of discrete water samples taken with the rosette sampler at the 68 CTD stations was measured by using the classical WINKLER procedure (e.g., Grasshoff et al. 1983). Titration was performed with a DMS Titrino 716 of METHRON AG. The end point of titration was determined potentiometrically. The accuracy of the method was ± 0.02 cm^3 dm^{-3}.

On two tracks a SEABIRD SBE 911+ CTD was towed with a ScanFish Mk II some hundred meters behind the research vessel, undulating in the depth range between 5 m and near the bottom or a maximum depth of about 170 m at a towing speed of 3.5 m s^{-1}. Additionally, a two-channel Haardt fluorometer was carried by the fish for measuring chlorophyll-*a* and backscattering intensity of emitted light.

Continuous underway measurements of surface temperature and surface salinity were made throughout the cruise. Seawater was pumped from a sea chest located in 4-m depth into a container lab located on the main deck. Temperature and salinity of the seawater were measured by a Seacat SBE 16 instrument with a sampling rate of 10 minutes. A linear correction function was derived from comparison measurements of 27 CTD-profiles on stations with a temperature variation of less than 0.01 K in the upper 10 m of the water column. The resulting mean error of the salinity is 0.01 psu and of temperature is 0.02 K, respectively.

Current was measured with a 300-kHz Direct Reading Broadband ADCP towed in 1-m depth on a small catamaran. Heading and position measurements of the catamaran were performed by an Attitude Determination Unit of AshTech (ADU II) with a four-antenna array attached to the catamaran. The catamaran was towed 150 m behind the ship on the leeward side of the wake of the research vessel in order to avoid hydrodynamical disturbances and to reduce short period pitch and roll motions by wind waves and swell. This towing position was also necessary to avoid multipath effects to the ADU II caused by reflections of satellite signals from the ships superstructure. The towing speed ranged between 3 and 3.5 m s^{-1}.

The depth range of the ADCP measurements was between 3 and 70 m. The averaging interval for the processed data was 600 s. During the cruise 10 tracks were performed in order to calibrate the ADCP and the ADU II over the continental shelf with bottom tracking mode. Scaling factor and alignment between ADCP and calibration data were calculated according to Joyce (1989), and the results are shown in Table 1.

TABLE 1. Results of ADCP calibration tracks.

Number of calibration tracks	Mean scaling factor	STD of scaling factor	Mean alignment in degree	STD of alignment
3	1.031	0.003	28.2	1.0
7	1.011	0.002	25.9	0.15

The raw ADCP data were quality checked using error velocity, vertical velocity, percent good, and correlation. The ADU II position measurements were quality checked with respect to velocity and acceleration of the ship. A comparison of validated ADCP measurements referenced to bottom tracking and satellite navigation was performed on the shelf off Swakopmund and the results are shown in Fig. 3.

The correlation coefficient between both current measurements is 0.8. The standard deviation of the difference between the velocity measurements referenced to global positioning satellites (GPS) and those referenced to bottom tracking is 5 cm s^{-1}. This may be accounted for by the accuracy of position measurement of the ADU corresponding to the accuracy of conventional GPS.

The wind vector was measured hourly by a ship Väisälä weather station. The cup anemometer and the wind vane were located at the top of the foremast 20 m above sea surface. Wind direction and wind speed derived from the NASA scatterometer (NSCAT) onboard the Japanese-built Advanced Earth Observing satellite (ADEOS) cover a larger area and permit a synoptic view. The data were kindly provided from the Physical Oceanography Distributed Active Archive Centre of the Jet Propulsion Laboratory (NASA) in half-degree averaged squares, adjusted to 10-m height. One dataset per day is available starting from 1 April 1997 and ending on 31 May 1997. It covers the region bounded by the longitudes 10°W to 20°E and latitudes 35°S to 5°N.

A quality check of the NSCAT data was performed by comparing direct measured wind vectors from three research vessels operating in the area covered by the received data. The correlation between NSCAT wind data and wind measurements on board the ships, shown in Fig. 4, is between 0.8 and 0.9, and the standard deviation of the difference between directly and satellite based wind measurements is 2.1 m s^{-1}. This is a surprisingly good agreement taking into account the difference in the averaging methods of both types of measurements.

From the 3-day average, wind stress values for each data point were calculated using the standard formula

$$\boldsymbol{\tau} = C_D \rho |\mathbf{W}| \mathbf{W},$$

where $\boldsymbol{\tau}$ is the wind stress vector, ρ is the density of air at 20°C (1.204 kg m^{-3}), **W** is the wind velocity adjusted to 10-m height and C_D the variable drag coefficient. The drag coefficient for a neutral atmosphere above the sea surface was chosen according to Smith (1988). Hereafter the wind stress curl was calculated for all points within the boundary of the area using a central difference method.

3. Results

a. *Horizontal structure of temperature, salinity, density, and current*

The distribution of sea surface temperature (SST) in 4-m depth shown in Fig. 5 depicts the 20°C isotherm at about 16°S. It separates a wide pattern of warm Angola Current water in the north from a narrow band of cold upwelling water located south of the ABF on the shelf. Within the Angola Current water a secondary front is found at 14°S both on the shelf as well as 200 km offshore. A relative maximum of SST stretches along the shelf edge north of the ABF suggesting a tongue-like structure of the Angola Current water. With-

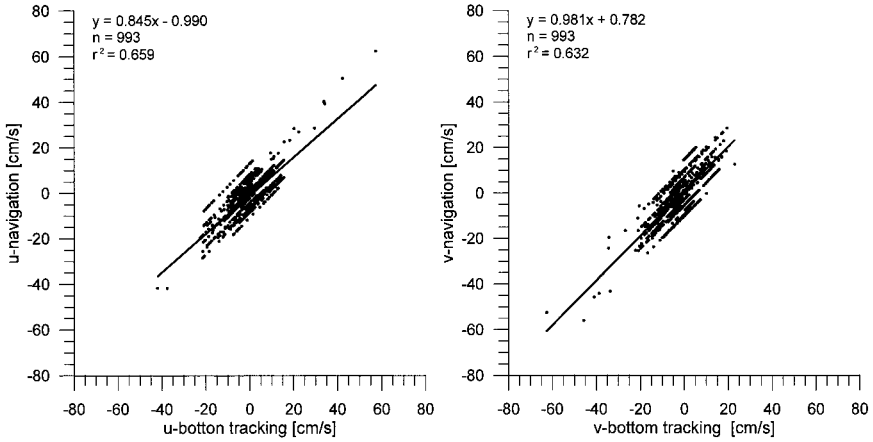

FIG. 3. Surface currents measured by towed ADCP with reference to bottom tracking and with reference to ADU II satellite navigation. The solid lines are the linear regression curves of current components referenced to satellite navigation versus bottom tracking.

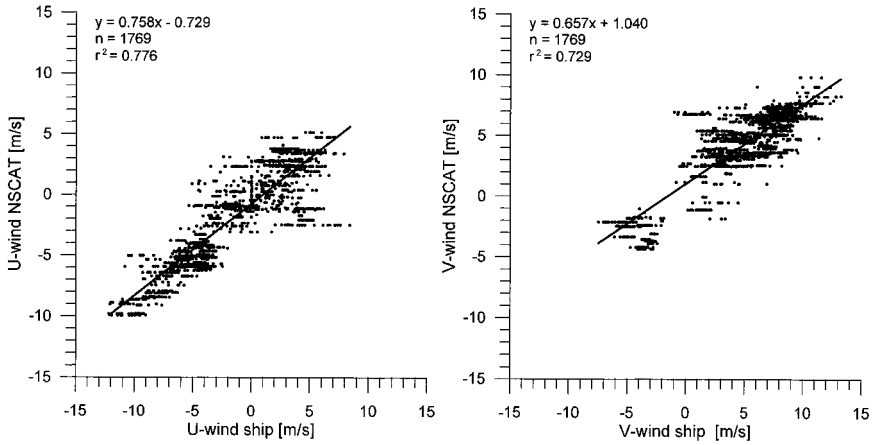

FIG. 4. Comparison of wind measured on board the R/V *Polarstern* (Julian day 92–103), R/V *Dr. Fridjof Nansen* (Julian day 107–112), and R/V *P. Kottzov* (Julian day 113–130) with simultaneously measured wind by the NSCAT. The solid lines are the linear regression curves of NSCAT wind versus ship measured wind components.

in the tongue, smaller structures with a length scale of 50 km are observed. However, with the measurements at hand it cannot be resolved whether the small structures are eddies or smaller tongues as described by Kostianoy (1996).

A second horizontal distribution of SST and sea surface salinity (SSS) was measured between 5 and 10 May 1997. The ABF did not significantly change its position between both legs of the cruise, but the axis of the tongue moved in an offshore direction and the SST of the near-shore water decreased (not shown here).

The SSS pattern, depicted in Fig. 5, reflects the distribution of both Angola Current water and upwelled water as well. Upwelling water south of the ABF and on the shelf has a SSS of less than 36 psu whereas the Angola Current water has usually a SSS in excess of 36 psu. A maximum of salinity is located at the shelf edge on the center section. In contrast to the SST pattern

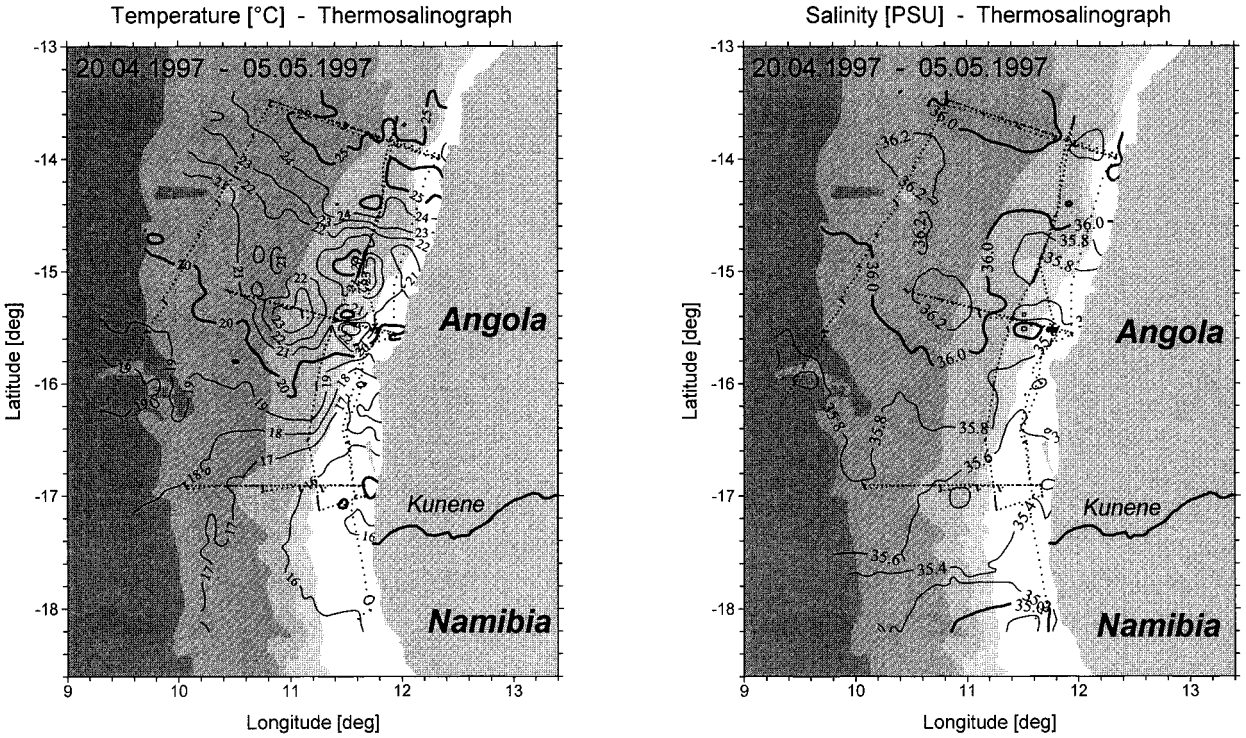

FIG. 5. Horizontal distribution in 4 m depth of sea surface temperature (left) and salinity (right) measured by a throughflow thermosalinograph. The thin dotted line indicates the ship track.

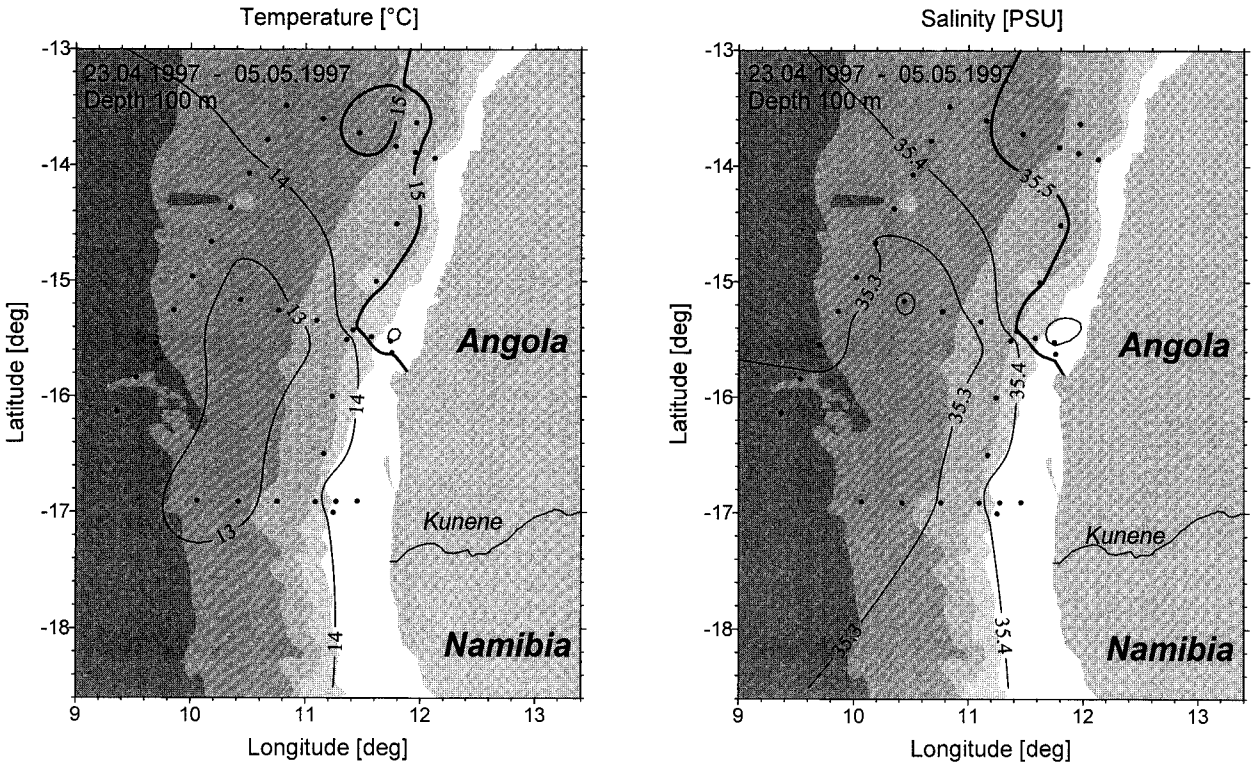

FIG. 6. Horizontal distribution of temperature (left) and salinity (right) in 100-m depth.

a SSS minimum is found at the shelf edge on the northern section suggesting a bifurcation of the salinity maximum toward north into an offshore branch and a second branch on the shelf. The salinity maximum extended more to the south during the second observational phase, and its near shore branch was separated from the coast by a 10-km wide band of less saline water. The density of the surface layer depicted the tongue-like structure of the SST as well. The density anomaly of the Angola Current water was less than 25.5 kg m^{-3} (not shown here).

A warm saline tongue of tropical Atlantic thermocline water, Gordon and Bosley (1991) also denoted as South Atlantic Central Water (SACW; e.g., Hagen 1991), is observed at deeper depth levels (see Fig. 6). The width of the tongue remains nearly 150 km at the northern cross section in depth levels below 50 m, but it is attached to the coast and its width decreases to a few tens of kilometers in a southward direction. The tropical Atlantic thermocline water was found on all stations of the area covered during the cruise except for the stations OS108 and OS109 (for location, see Fig. 2). This means that this water mass extended more to the south than the Angola Current water at the surface. The water mass at the stations OS108 and OS109 had a salinity lowered by 0.1 psu compared with the SACW. The latter water mass was found by Gordon and Bosley (1991) south of the Angola–Benguela front.

The horizontal distribution of surface currents is shown in Fig. 7. The surface current along both the offshore section and the southern section depict a well-developed westward component, which may be due to the Ekman Current. The longshore component of the surface current in the Angola Current water (northern section) is northward directed in an area extending from the coast to about 50 nm offshore followed by a southward-directed current farther offshore. The longshore current is southward directed over the full length of both sections the central one in the front area and the southern one in the Benguela water. These observed surface current pattern seems to be stable within a week as shown by repeated current measurements in Fig. 7 (right panel). It would fit into the scheme of the surface circulation described by Moroshkin et al. (1970), Gordon and Bosley (1991), and Shannon and Nelson (1996) if the cyclonic gyre centered at 12°S and 5°W is assumed to be deformed elliptically with an orientation of the major axis southeast to northwest during the phase of the observations described here.

b. Vertical structure of temperature, salinity, oxygen, and current

The vertical structure of potential temperature, salinity, and oxygen on the northern cross section down to a maximum depth of 1200 m are shown in Fig. 8.

A sharp pycnocline is observed in a depth of 30 m throughout the section except in a 20-km wide coastal

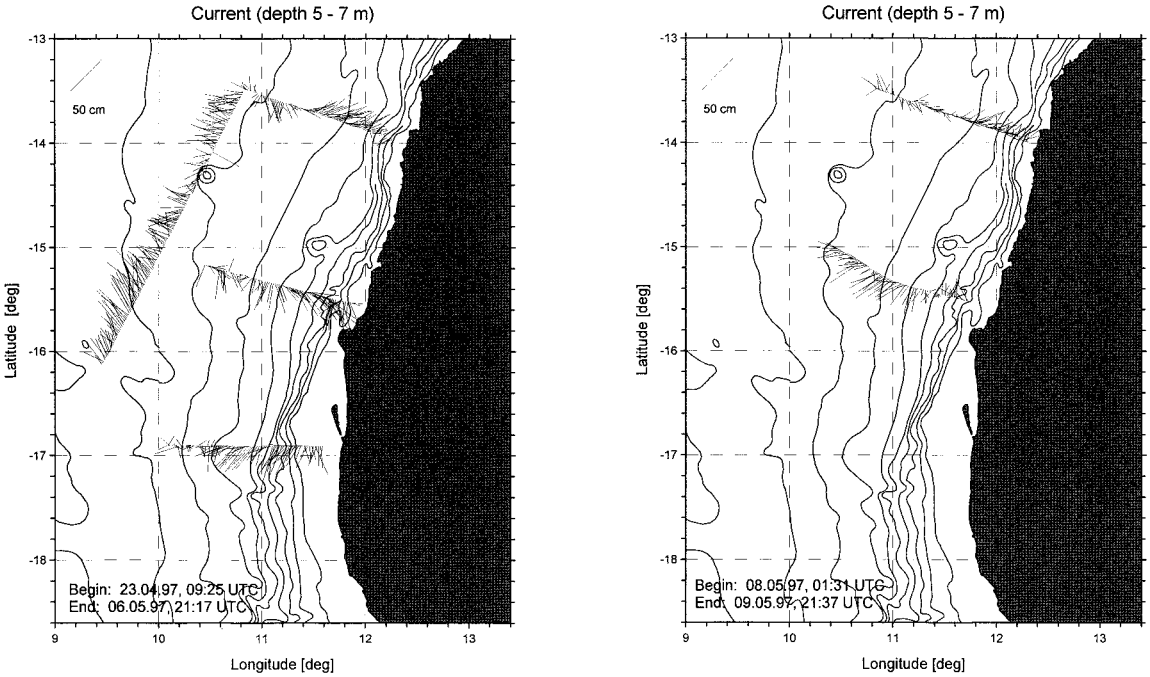

FIG. 7. Surface currents measured by towed ADCP with reference to ADU II satellite navigation. Repeated measurements right.

boundary layer where the pycnocline fans out. In the upper mixed layer, warm Angola Current water is observed with temperature in excess of 24°C apart from the coastal boundary layer where upwelling occurred which intensified between 3 and 7 May 1997. Salinity measurements revealed a jet like pattern of about 40-km width with maximum salinity of more than 36.4 psu at the shelf break.

Below the pycnocline wave like vertical displacements of isolines are observed with a horizontal scale of about 100 km. Oxygen depleted water of less than 2 $cm^3\ dm^{-3}$ is found between 700-m depth and the pycnocline with a core layer of less than 1 $cm^3\ dm^{-3}$ oxygen between 500- and 200-m depth. The core layer of the AAIW is found in 800-m depth with a minimum salinity between 34.5 and 34.6 psu.

On the central section, shown in Fig. 9, the pycnocline is quite similar as on the northern section aside from dome like upward bending centered at 50 km offshore with a horizontal scale of about 30 km. In the centre of this feature the pycnocline is as shallow as 10-m depth. The temperature in the surface mixed layer is 22°–23°C and the maximum salinity ranges between 36.3 and 36.4 psu about 150 km offshore. Upwelling occurs in a narrow coastal boundary layer as on the northern section. Here a water mass was found, which is characteristic for the shelf waters of the Benguela (e.g., Shannon and Nelson 1996). Strong downwelling was observed at the shelf edge in the depth range between the thermocline and a depth of about 500 m (downwelling is masked in the lower part of Fig. 9 by the 6-times compressed vertical scale). The distribution of water with oxygen of less than 2 $cm^3\ dm^{-3}$ is quite similar to those of the northern section. However, the upper bound of the low oxygen core is well above 200-m depth and extends at 30 and 120 km offshore distance just below the thermocline. The core layer of the AAIW was found at a depth of 800 m with salinity ranging between 34.5 and 34.6 psu. A small core of salinity below 34.5 psu is observed at 100 km offshore within the AAIW layer.

The vertical structures of temperature, salinity, and oxygen, as well as fluorescence, and backscattering on the southern section, are shown in Figs. 10 and 11, respectively. The pycnocline on this section is found well defined off 120 km offshore in a depth of 40 m but weaker than on the northern sections. Toward the shelf edge the pycnocline fans out by downwelling and upwelling processes and disappears on the shelf completely.

The whole surface mixed layer is covered by cold Benguela water with salinity below 35.7 psu. Upwelling of tropical Atlantic thermocline water with temperature of about 15°C and a salinity of 35.5 psu is suggested by the upward bending isolines in the upper 100 m at the shelf edge and on the shelf. This is supported by pattern of fluorescence in the chlorophyll-*a* range and backscattering of light, which both have a strong signal in the surface layer with a maximum at the very shelf edge. The signal of fluorescence in the chlorophyll-a range decreases rapidly with depth in contrast to the signal of backscattered light, which has an offshore gradient independent of depth below the thermocline. How-

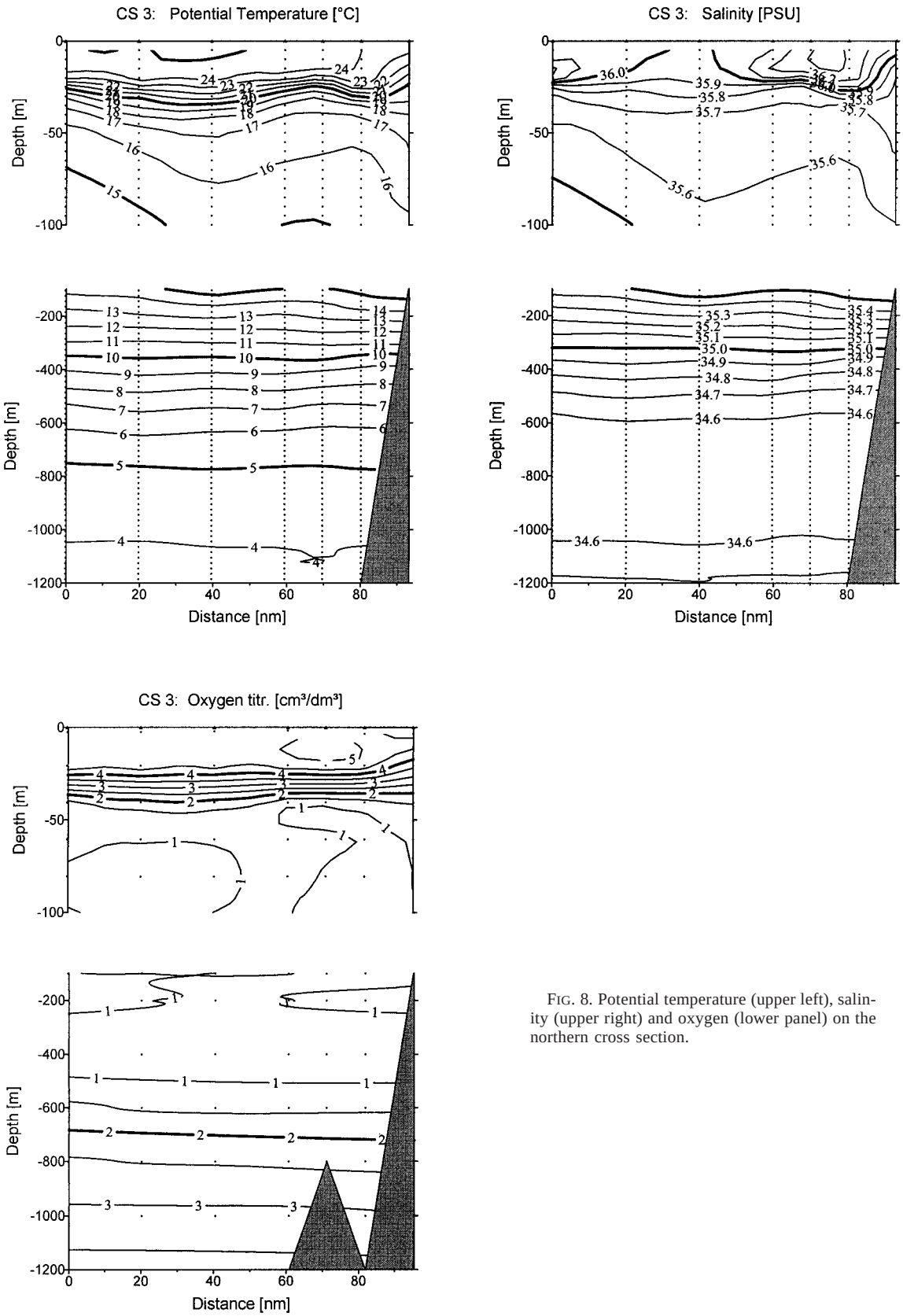

FIG. 8. Potential temperature (upper left), salinity (upper right) and oxygen (lower panel) on the northern cross section.

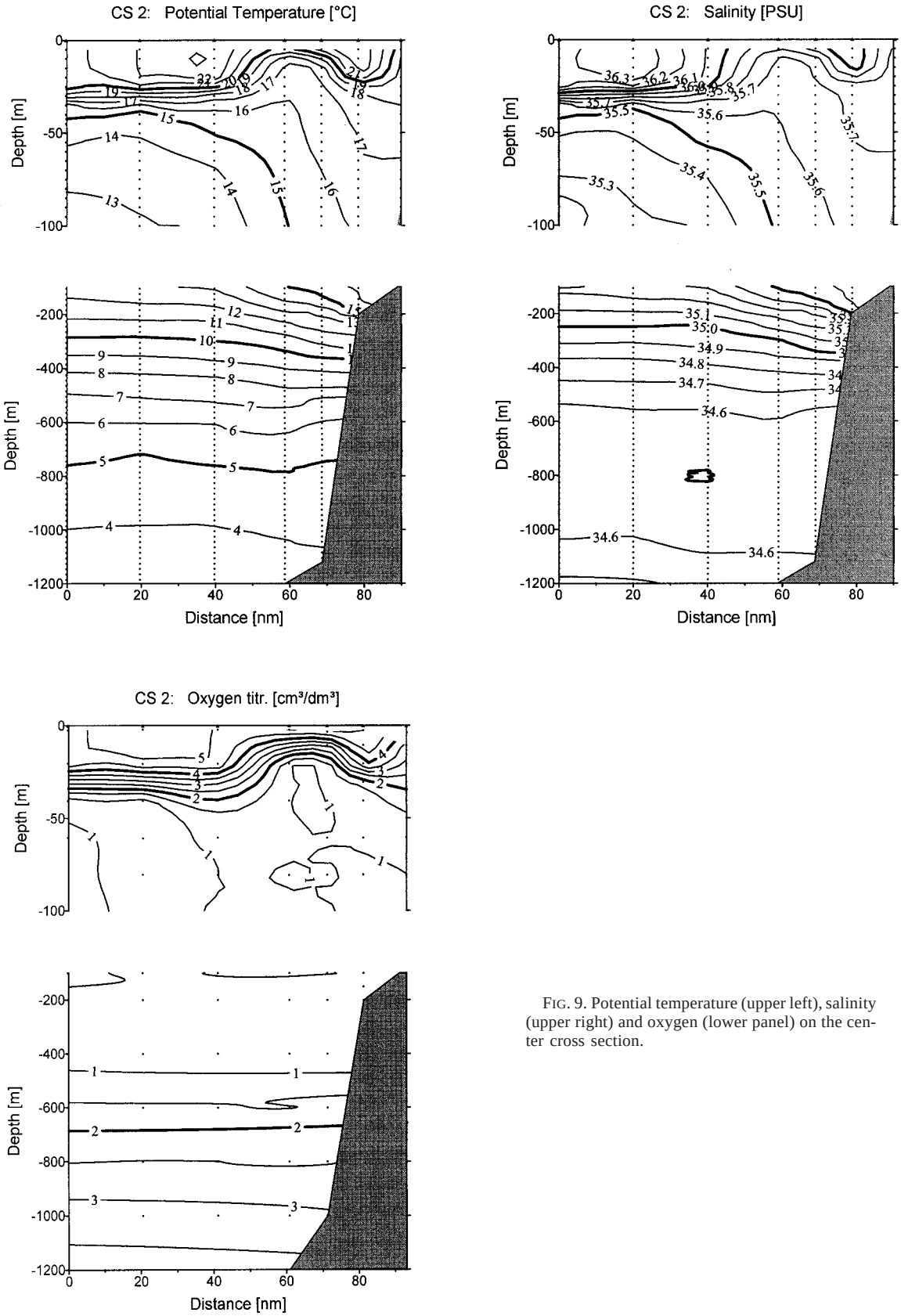

FIG. 9. Potential temperature (upper left), salinity (upper right) and oxygen (lower panel) on the center cross section.

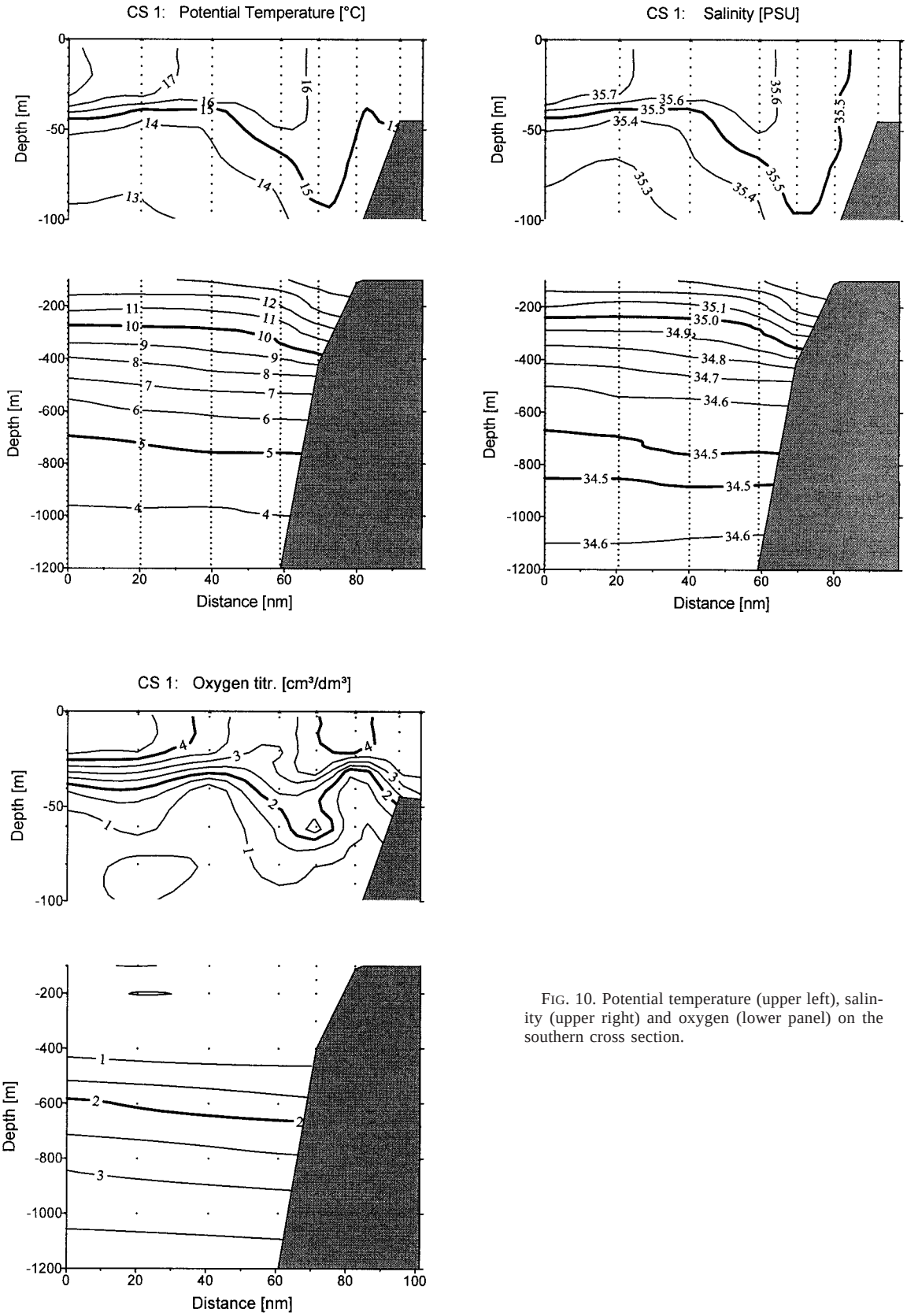

FIG. 10. Potential temperature (upper left), salinity (upper right) and oxygen (lower panel) on the southern cross section.

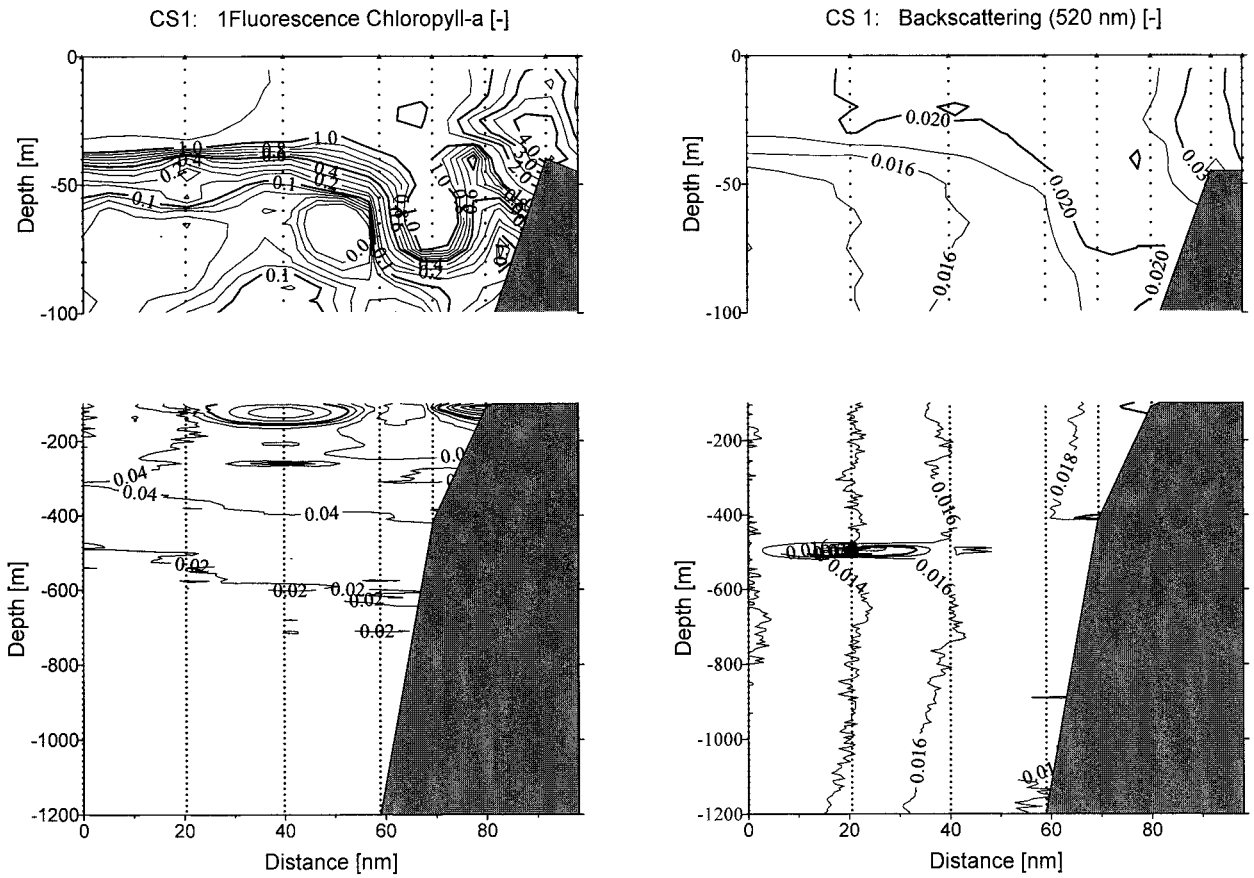

FIG. 11. Fluorescence (left) and back scattered light intensity (right) on the southern cross section.

ever, this gradient is not to be seen in the towed CTD measurements where the same fluorometer has been used. This discrepancy could be due to the two days difference in time between both sections. An instrumental error can not be excluded completely.

Both the potential temperature and salinity pattern indicate downwelling in a depth range between 100 and 500 m within a boundary layer of about 30-km width off the shelf break (take into consideration the different vertical scales of Fig. 10).

The layer of oxygen depleted water (<2 cm^3 dm^{-3}) is found between 600-m depth and the thermocline. Water with oxygen content below 1 cm^3 dm^{-3} extends between 400-m depth and the thermocline and contains some small patches with oxygen concentration below 0.5 cm^3 dm^{-3} in 200- and 100-m depth. The core layer of the Antarctic Intermediate Water (AAIW) with salinity less than 34.5 psu is in a depth between 850 to 700 m. The vertical core width decreases somewhat toward the shelf.

The near surface pattern on the southern cross section is resolved in more detail by the towed CTD measurements depicted in Fig. 12. The upper layer of the ocean is characterized by a pycnocline at 40-m depth, which separates a deep layer with water of less than 15°C and a salinity below 35.5 psu from an upper layer with warmer and saltier water. The pycnocline is subject to vertical excursions with an amplitude of about 15 m and a wavelength of 20 km. It begins to disperse at the shelf edge, which can be accounted for by the action of downwelling below 60-m depth and upwelling above this depth. Upwelling provides cold (15°–16°C) and less saline (35.5–35.6 psu) water on the shelf, which gradually increases in both temperature and salinity in offshore direction within the upper mixed layer. On the shelf and in the upper mixed layer, fluorescence and back scattered light have maximum values, but in contrast to temperature and salinity both have a patchy structure there (see Fig. 12). This implies that the biological sources have a shorter timescale than the timescale of the mixing processes.

A typical feature of the upper mixed layer on the southern section is the separation of water bodies in offshore direction by almost vertical fronts. This mixing may be a result of differential advection due to the interaction between the vertical current shear of the Ekman offshore current in the surface layer and the compensating onshore current below the thermocline and the offshore component of the density gradient (see van Aken 1986).

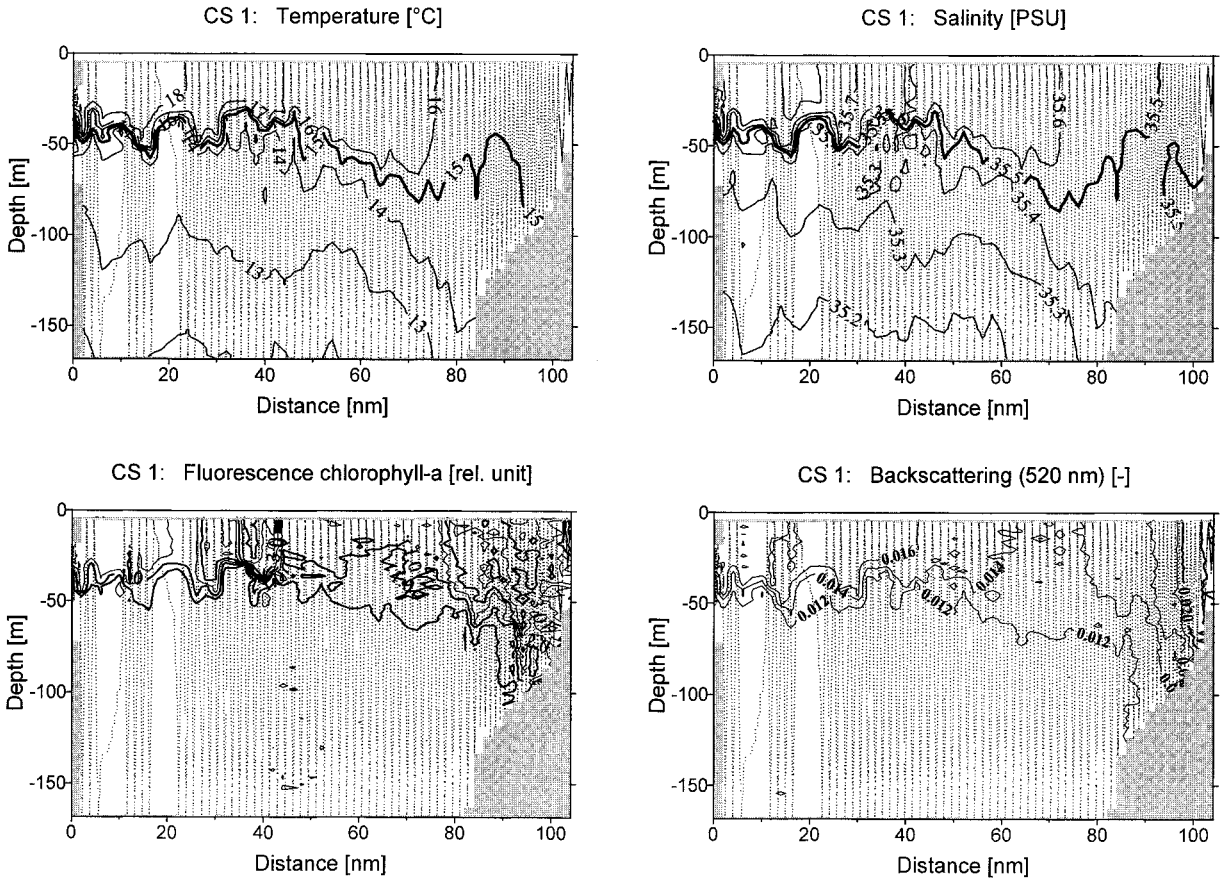

FIG. 12. High resolution distribution of temperature (upper panel, left), salinity (upper panel, right), fluorescence (lower panel, left), and back scattered light (lower panel, right) measured by towed CTD.

The vertical structure of the meridional current component on the cross sections is shown in Fig. 13. On the northern section the northward flowing current is embedded between 20 nm and 100 km offshore distance in the upper 50 m in a deep reaching southward flow. The maximum value of northward flow is observed near the sea surface about 90 km offshore. The maximum southward current was measured at the western rim of the section.

On both the central and the southern cross section generally southward flowing currents are observed. These current patterns are deep reaching as well and do not appear to be correlated with the thermocline. Maximum southward flow is located at the shelf edge on both sections. However, the southward flow is more intense on the central section than on the southern one.

The vertical structure of the temperature and the salinity on the longitudinal section located at about 150 km off the coast is shown in Fig. 14. The thermocline is inclined from 20-m depth in the north to 40-m depth in the south. A domelike pattern with a similar horizontal scale as those found on the central cross-shore section is observed at 100-km distance from the northern edge. The doming of the isotherms and isohalines extends from the mixed layer to at least 300-m depth. Angola Current water with temperature above 24°C and salinity of 36.3 psu is found at the northern edge of the section. This water gradually becomes colder and less salty in a southward direction. The depth of both isotherms and isohalines decrease between 13.5° and 15.5°S in the depth range of 600 to 100 m but are not inclined south of 15.5°S. Wavelike vertical displacements with wavelength of 100 km are observed in the upper 300 m.

Oxygen depleted water (<2 cm^3 dm^{-3}) is found between 700-m depth and the thermocline in the north. The upper bound deepens to about 120-m depth in the south of the section. Water with less than 1 cm^3 dm^{-3} oxygen concentration is observed in the layer between 500- and 200-m depth. A doming of the upper bound of this layer with its center well south of the corresponding doming of the temperature pattern can be recognized. The core layer of the AAIW is found at about 800-m depth along the whole section but the salinity increases in a northward direction.

The east component of the current on the longitudinal section is shown in Fig. 15. Generally westward flow with about 0.15 m s^{-1} is observed in the upper mixed

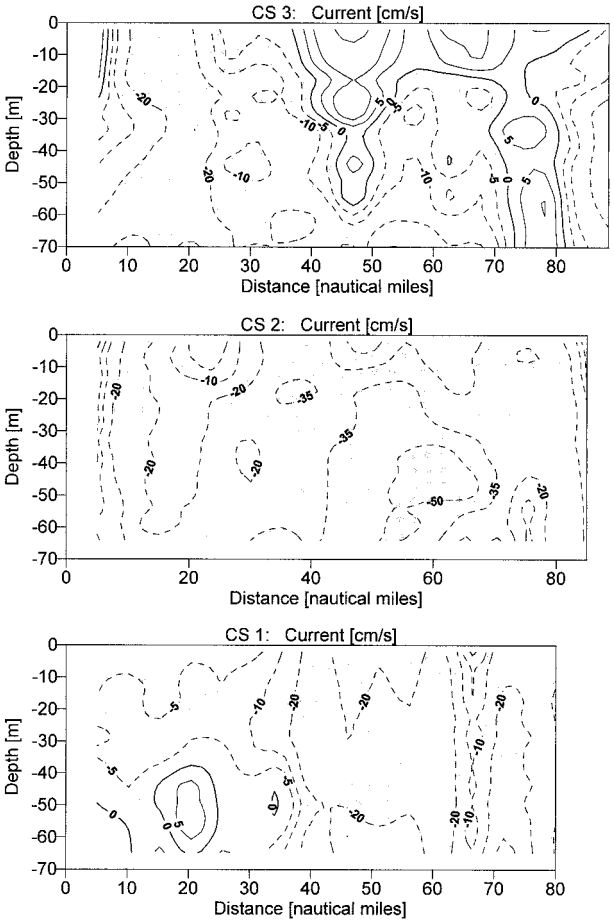

FIG. 13. North component of current on cross sections measured by towed ADCP with reference to ADU II satellite navigation.

layer. Interpreting this as an Ekman Current and integrating from the surface to the depth of the thermocline and along the whole section this amounts to a westward Ekman transport of about 1.3 Sv in the upper mixed layer. This is an overestimation since the mean Ekman offshore transport through the section calculated from the mean wind velocity of the cruise was 0.9 Sv. However, taking into account the estimated error of the ADCP of 5 cm s^{-1} the uncertainty of the measured Ekman transport above the thermocline amounts to 0.6 Sv along the section. This suggests that the westward directed Ekman Current is a significant fraction of the current measured by the ADCP in the surface mixed layer of the section. Below the thermocline, a broad deep extending eastward flow band expands between 60 to 220 km from the northern edge of the section. The maximum of the eastward flow is measured at the northward rim of the dome like pattern.

c. Dynamic depth topography and geostrophic currents

Dynamic depth anomalies have been calculated at every CTD station by means of Seasoft of SBE. In order to obtain a unique reference level at 1200 dbar a technique described by Defant (1961) has been employed to extrapolate the dynamic depth anomalies below the bottom on stations with a bottom depth shallower than 1200 dbar. This technique is based on the assumption of no geostrophic flow below the sea bottom.

The dynamic topographies at 0 and 100 dbar with reference to 1200 dbar are depicted in Fig. 16. The most obvious feature is a narrow belt of a strong gradient in the topography located at the transition between the plateau of the sea level elevation in the north eastern and the south western area covered by the station grid. The north eastern plateau is about 10 cm higher than the flat area located offshore in southwesterly direction. The upper plateau is becoming significantly narrower and slightly decreasing in height while stretching southward along the coast. The dynamic topography at the 100-dbar level shows the same pattern as at the sea surface. However, the elevation is a few centimetres smaller.

Geostrophic currents have been calculated with reference to 1200 dbar on the sections. The vertical pattern of geostrophic currents on the northern and central sections are shown in Fig. 17. On the northern cross section a geostrophic northward flow is embedded in the center of this section into a southward flow. On the central cross section, a jet-like southward flow in the upper 200 m is observed that has a double core structure. One core is located on the shelf the other is located about 50 km offshore at the shelf edge. A southward directed geostrophic jet with a single core is observed on the southern section. The core of the jet is located at the shelf break and extends down to 200-m depth (see Fig. 18).

The geostrophic current on the longitudinal section is shown in Fig. 18. In the northern 200 km of the section an eastward geostrophic flow is observed interrupted by a small band of westward flow in the vicinity of the dome-like pattern in potential temperature and salinity (cf. with Fig. 14). In the southern part of the section, westward flow is observed in the upper 200 m.

The general structure of the geostrophic flow agrees with those of the direct measured currents on the sections except in the upper mixed layer of the offshore section. Here the geostrophic current seems to be masked by the stronger Ekman Current.

Geostrophic transports normal to the sections have been calculated between the sea surface and the 1200-dbar level. The transport through the area stretched by the westernmost stations of the cross sections amounts to 5.4 Sv directed toward the coast between the northern and the central cross section and to 0.6 Sv between the central and the southern section. The transport through the northern cross section is about 1 Sv southward. This sums up to a transport of 7 Sv directed into the box formed by the southern and northern cross section. A southward transport of 7 Sv is leaving the box through the southern section. The geostrophic volume flow is balanced in first order (see Fig. 19).

The Ekman offshore transport in the surface mixed

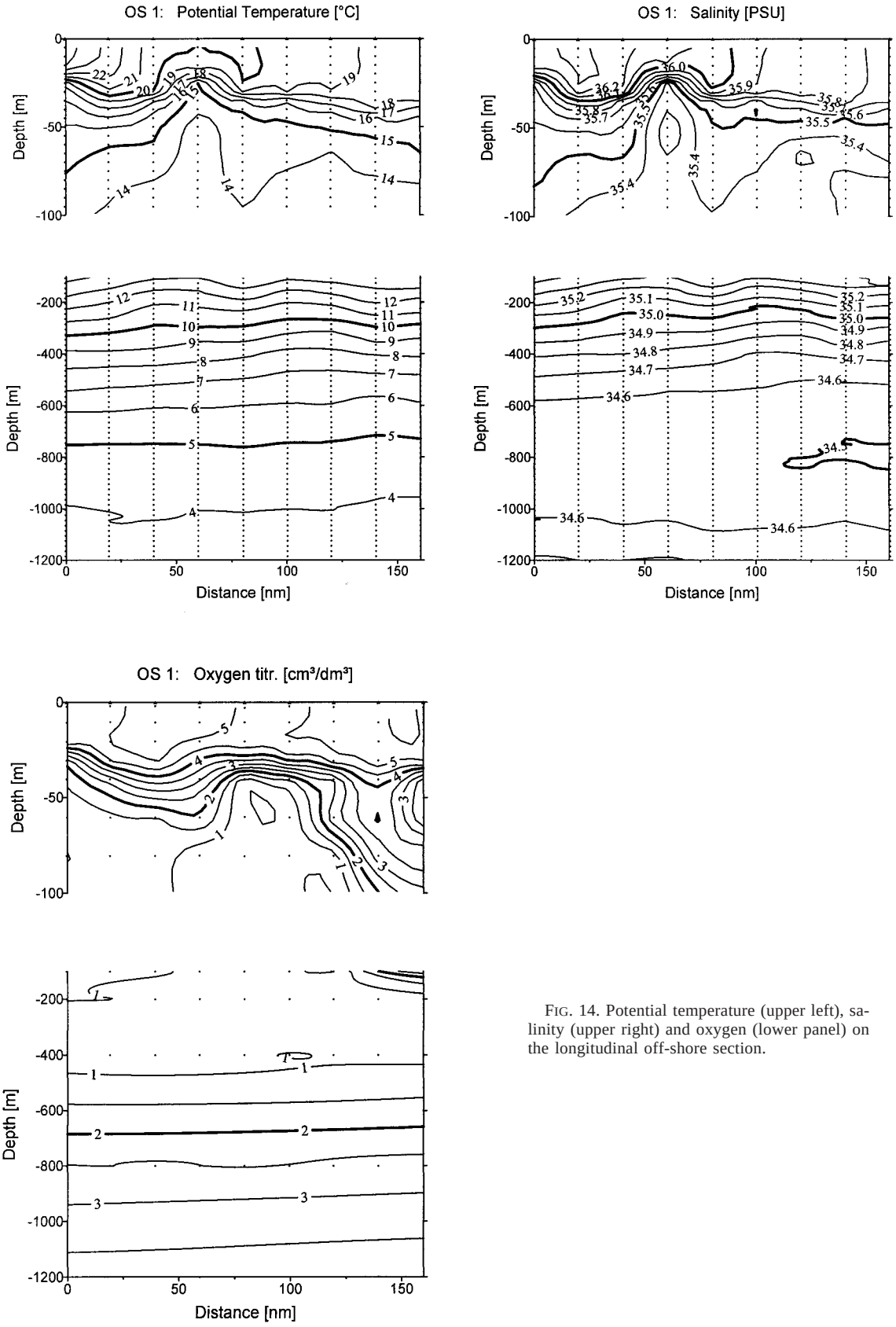

FIG. 14. Potential temperature (upper left), salinity (upper right) and oxygen (lower panel) on the longitudinal off-shore section.

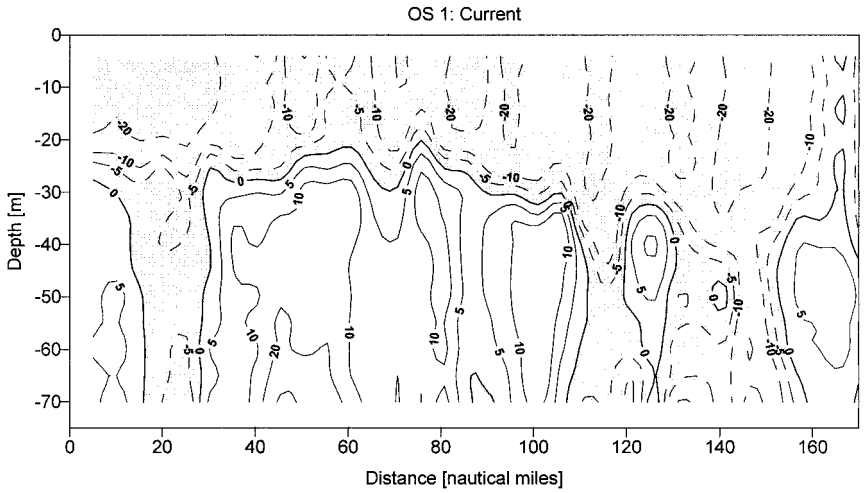

FIG. 15. East component of current on the longitudinal off-shore section measured by towed ADCP with reference to ADU II satellite navigation.

layer does not affect the mass balance described above since it is being compensated by a barotropic current such that the resulting mass transport normal to the coast vanishes (e.g., Fennel and Lass 1989). This compensation occurs within a coastal boundary layer of one barotropic Rossby radius. The compensating current below the surface layer cannot be measured directly since it is much weaker than the error bounds of the instrument. Moreover, the compensating deep current cannot be found from a geostrophic analysis assuming a level of no motion.

d. Spatial structure of the wind field

Wind vectors and windstress curl derived from NSCAT measurements have been averaged at the grid points for three consecutive 20-day periods from 1 April to 31 May 1997 covering the cruise of R/V *Dr. Fridjof Nansen*, the cruise of R/V *Peter Kottzov* (see Fig. 20), and the post-cruise period from 11 to 31 May 1997. The 20-day averaging time has been selected since it is roughly the duration of the cruises and the significant quasi-synoptic structures observed in the water column during the cruise are likely to be excited by atmospheric processes of a comparable timescale.

The observed mean wind field during the three periods is quite stable depicting typical features of the atmospheric circulation over the ocean in subtropical and tropical latitudes as described by Hellerman and Rosenstein (1983). This comprises the monsoon in the Gulf of Guinea between 5°N and 5°S, the belt of southeast trades between 5° and 25°S, and the zone of calm winds in the center of the subtropical anticyclone. The associated pattern of windstress curl is characterized by positive (anticyclonic) values between 35° and 15°S associated with the meridional gradient of the zonal wind component between the west wind belt and the southeast trade belt. The corresponding downwelling by the convergence of the Ekman transport forces the Benguela current as a branch of the subtropical gyre. Between the latitudes of 15° and 5°S generally low values of the windstress curl are observed.

Persistent negative (cyclonic) wind stress curl has been derived from the measured wind field in the equatorial belt of the eastern Atlantic between $\pm 5°$ latitude.

The wind field pattern in the coastal zone resembles in several points those described by Bakun and Nelson (1991). It is characterized by a predominantly northward (upwelling favorable on the Southern Hemisphere) directed windstress along the whole African coast from the Cape of Good Hope to the Gulf of Guinea. Generally the strength of the northward directed wind decreases toward the meridionally aligned coast of Africa, implying negative (cyclonic) wind stress curl.

A 300–400-km wide belt of negative wind stress curl resides along the coast from Cape Town up to at least 15°S. Within this belt the cyclonic wind stress curl depicts a patchy distribution in particular during the first and the third averaging period. Distinct cells are observed near Cape Frio, between Lüderitz and Walvis Bay, and near Cape Columbine as described by, for example, Boyd (1987). The poleward limit of this belt is near Cape of Good Hope in April and early May and moved toward the equator in late May in agreement with the seasonal cycle described by Bakun and Nelson (1991).

In contrast to Bakun and Nelson (1991), we do not observe an area of anticyclonic wind stress curl at the equatorial limit of the belt of cyclonic wind stress curl. Rather an extension of this belt was observed stretching toward north west into the open ocean north of 15°S. This extension is quite variable within a timescale of about three weeks. During the first in early April 1997 this continuation into the open ocean is marginally only. In the phase from 20 April to 10 May it is well exhibited,

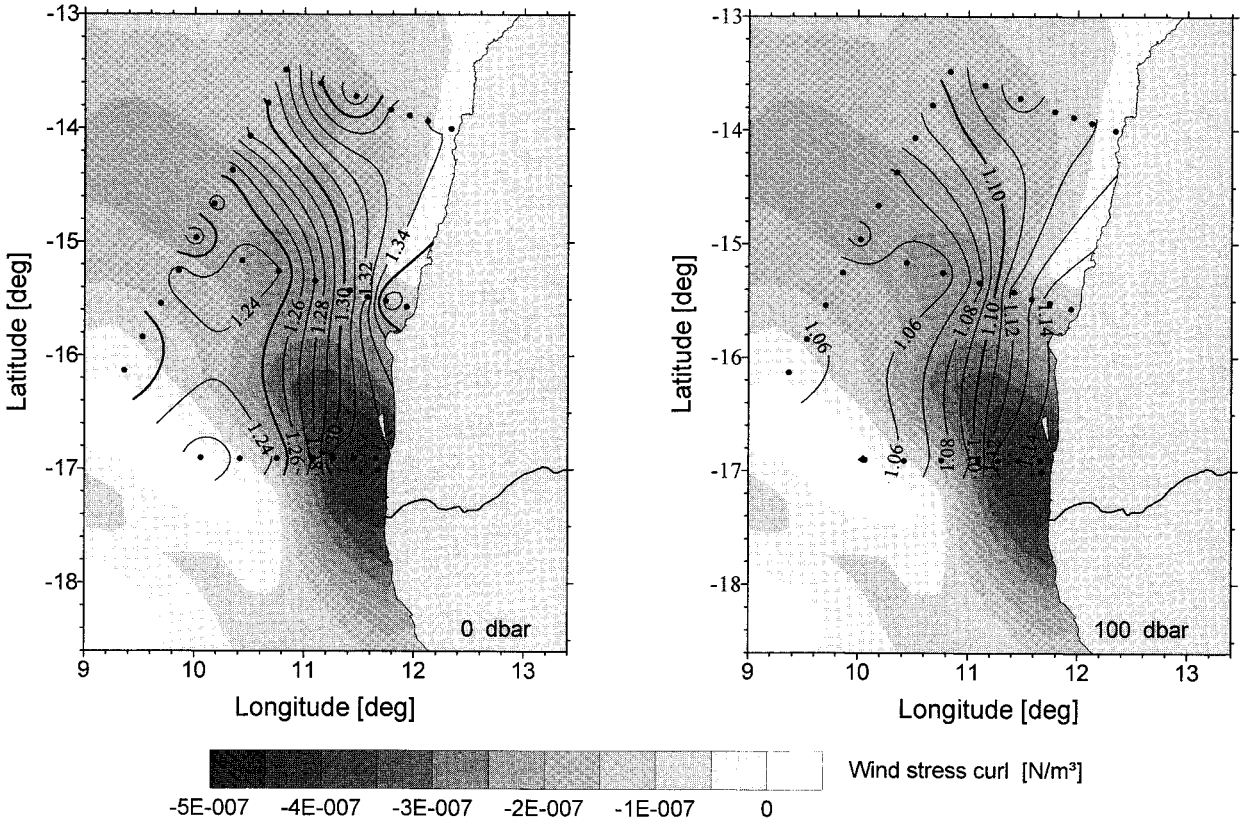

FIG. 16. Dynamic topography at 0 dbar (left) and 100 dbar (right) with reference to 1200 dbar. The wind stress curl averaged in time from 20 April to 10 May 1997 is depicted as shading in a grey scale.

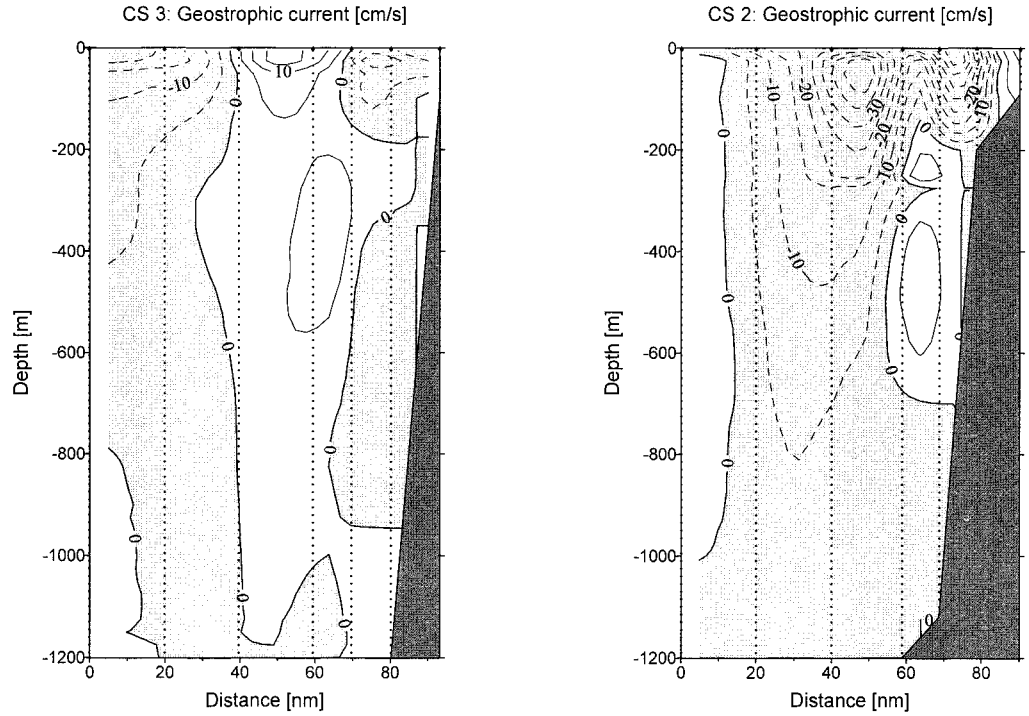

FIG. 17. Vertical distribution of geostrophic current with reference to 1200 dbar on the northern (left) and center (right) cross section.

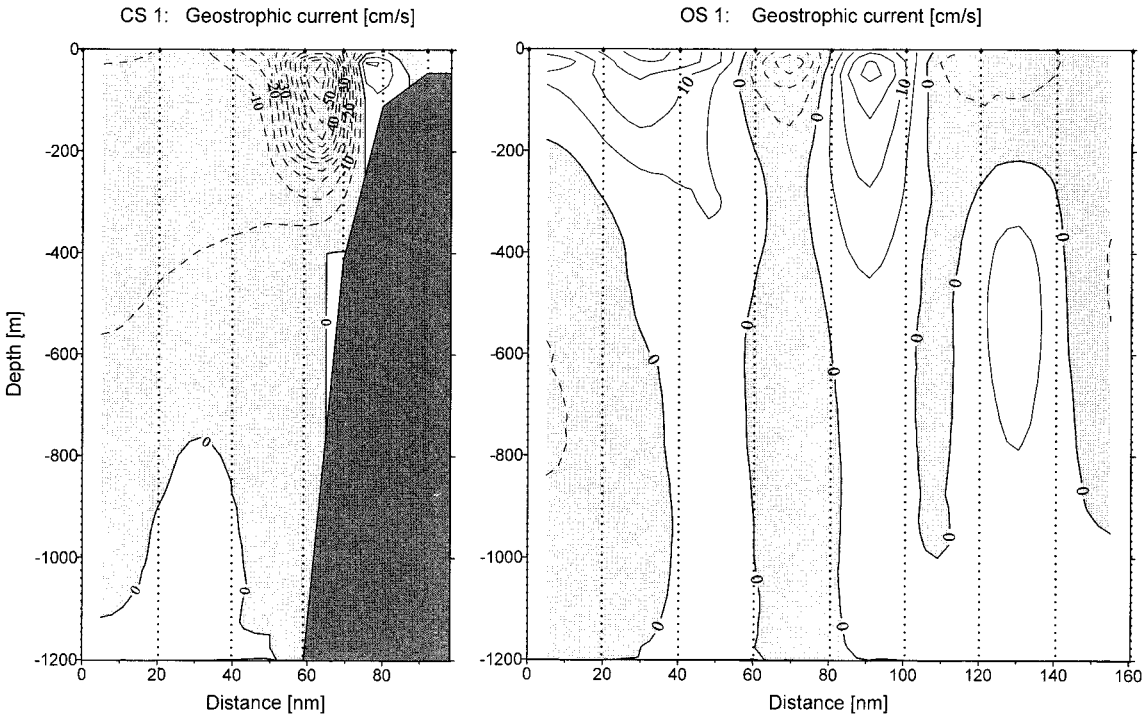

FIG. 18. Vertical distribution of geostrophic current with reference to 1200 dbar on the southern cross section (left) and the longitudinal offshore section (right).

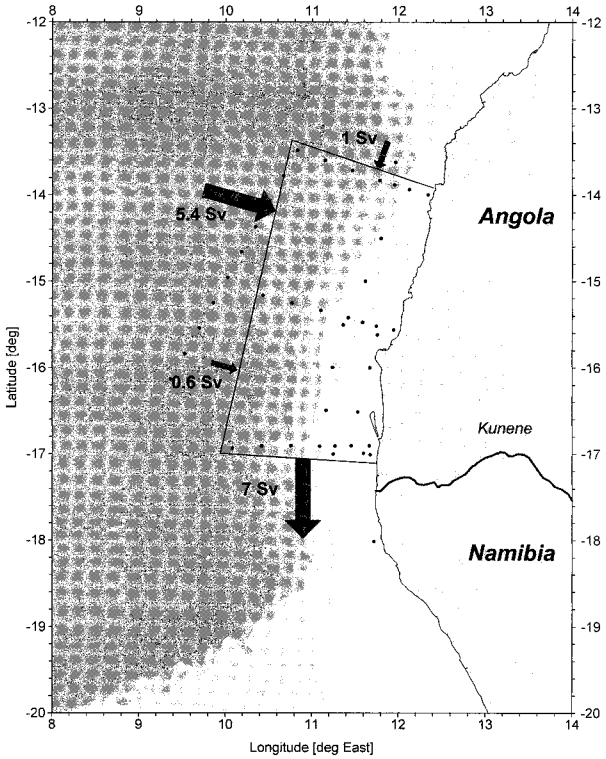

FIG. 19. First order mass balance in the Angola–Benguela front area between 20 April and 12 May 1997.

at least up to 10°S, and merges into the equatorial zone of negative wind stress curl (see Fig. 20). During 10 to 30 May 1997 the extension of the belt into the open ocean disappeared and it is divided into a few separated plumes.

4. Discussion

The hydrographic pattern in the surface mixed layer observed during 20 April to 12 May 1997 agree well with those of the Angola–Benguela front described by Shannon et al. (1987) and Meeuwis and Lutjeharms (1990) according to the season of the year. The front, characterized by the 20°C isotherm was located at 16°S at the sea surface. It separated a 30–40-m thick tongue of warm and saline Angola Current water from cold and less saline Benguela water. The pattern of SSS branched within the tongue into one filament of higher salinity stretching northward along the coast and into a second filament extending toward the northwest, into the open ocean. The width of the tongue decreased southward from more than 200 km at 13°30′S to 100 km at 15°30′S. The warm water was separated from the coast by a thin belt of colder, possibly upwelled water. The width of this coastal boundary layer increased southward and the water within the boundary layer merged with the Benguela water south of the front at 16°30′S. The temperature gradient within the front area was about 5 K per 2° of latitude which is weaker than usual according to Shannon et al. (1987). The general pattern of the Angola

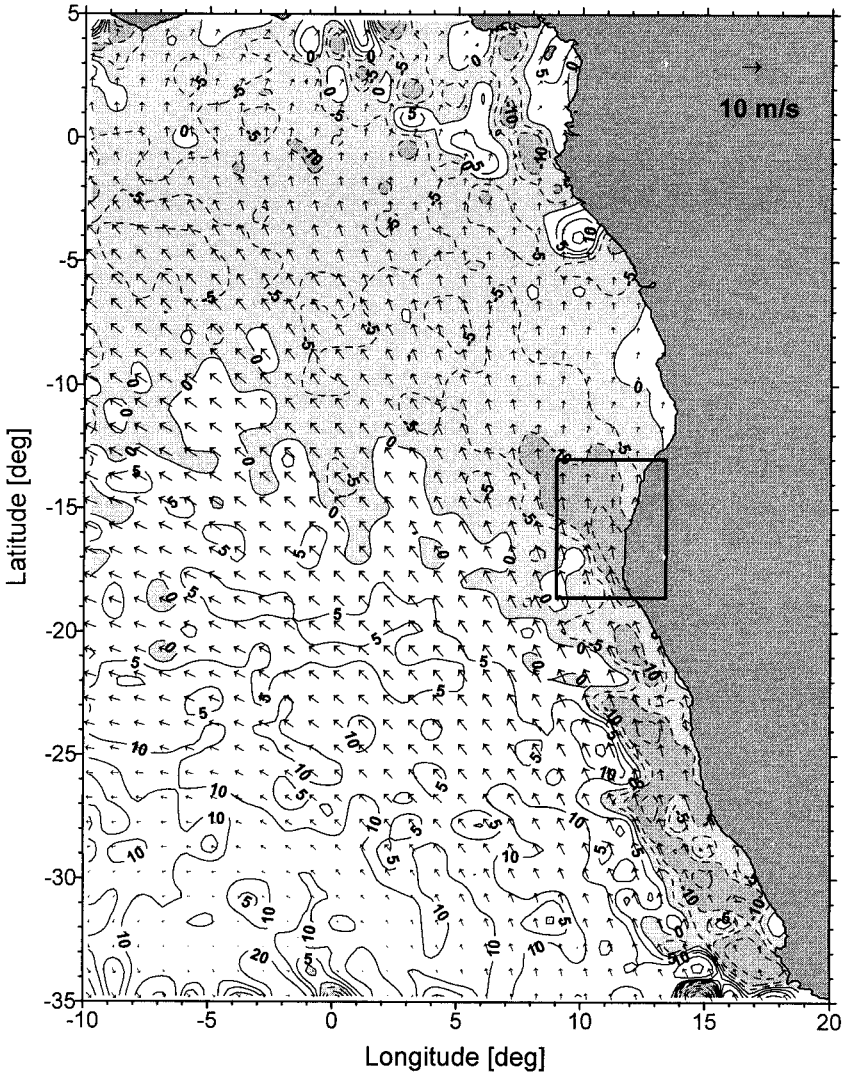

FIG. 20. Wind vector and contour lines of windstress curl (10^{-8}N m^{-3}) derived from NSCAT measurements averaged over 20 April to 10 May 1997. The square at the coast indicates the area of investigation during the cruise.

Current water agrees well with the pattern observed by R/V *F. Nansen* during the first half of April (Gammelsrod et al. 1997). However, at this time the ABF was displaced more to the south, namely at 17°S.

Below the mixed layer tropical Atlantic thermocline water was observed in the whole area studied except for two stations in the south-western corner of the area and for some stations right on the shelf, respectively. On these stations, a less saline water mass was observed, which is characteristic for the upwelling in the Benguela (see Shannon and Nelson 1996), and which was found by Gordon and Bosley (1991) south of the Angola–Benguela front. On the other hand, the tropical Atlantic thermocline water sometimes extends along the shelf edge as far south as 27°S, Gordon et al. (1995). The pattern of the horizontal distribution of temperature and salinity below the mixed layer consisted of a broad plateau of warm and saline water north of about 14°S. This water was separated from cooler and less saline water between 15° and 17°S with a center located at least 150 km offshore. The warm and saline water found in the north continued as a narrow band along the shelf edge to eat least 17°S, which was associated with intensive downwelling in the depth range between the base of the mixed layer and 500-m depth on the sections at 15°S, CS2, and 17°S, CS1, respectively. The relation between the pattern of temperature and the pattern of the wind stress curl will be discussed below.

Oxygen depleted water (<2 cm^3 dm^{-3}) was observed in the depth range between 700 m under the lower rim of the thermocline in the whole area bounded by 13.5° to 17°S and the coast to 10°W. Water with oxygen concentration of less than 1 cm^3 dm^{-3} was found in the same area between about 500-m depth and at least

200-m depth. The upper bound of this water extended uniformly to the lower thermocline south of the Angola–Benguela front. Here patches of water were observed between 200 and 100 m depth containing oxygen concentration below 0.5 $cm^3\ dm^{-3}$. North of the front the upper bound of the 1 $cm^3\ dm^{-3}$ oxygen concentration was found significantly deeper in the mean than south of the front. Taking into account the observed current pattern this indicates that oxygen depleted water between 700- and 200-m depth was advected poleward along the coast from the pool of oxygen depleted water located in the area of the Angola Dome as described by Bubnov (1972) and Chapman and Shannon (1985). The southward extension of water masses with low oxygen content is well emerged in the third and fourth quarter of the year but starts to develop already in the second quarter (Chapman and Shannon 1987). The oxygen distribution in the upper 200 m suggests that oxygen consumption by remineralisation of sinking particulate organic material is intensified south of the Angola–Benguela front due to the higher productivity.

The core of the AAIW was observed in about 800-m depth in the whole area of observation. The salinity minimum was about 34.50 psu at 15°30′S increasing toward the equator. This fits well into the basin wide increase of AAIW core salinity toward east and north, respectively, as described by Shannon and Hunter (1988) and Boebel et al. (1997). Generally, the core salinity of the AAIW was higher at the shelf edge than some 20 km offshore as described by Duncombe Rae (1998). This is in agreement with a poleward flow of AAIW water of higher core salinity at the shelf edge according to Shannon and Hunter (1988). However, the fine structure of the 34.4 psu isohaline was observed to be cusps like directed from the southwest corner of the station grid toward northeast. The center of the cusp was located about 120 km off the shelf edge. This suggests that a small band of AAIW water with lower core salinity is flowing as an equatorward counter current off shore from the poleward flow of AAIW water with higher core salinity located right at the shelf edge. Similar indications were found by Shannon and Hunter (1988) in the southern Benguela.

The pattern of dynamic topography with respect to the 1200-dbar level resembles those of temperature and salinity in the thermocline. A plateau of positive sea level elevation of about 10 cm extending offshore by more than 150 km was found north of 14°S. This plateau spread southward along the shelf to at least 17°S. A trough in the dynamic topography of the sea surface extended roughly from 15°S, 10°E toward south with the talweg at an offshore distance of about 150 km. The positions of the talweg are close to the positions of the minimum in the wind stress curl (see Fig. 16). This suggests that the dynamic topography of the sea surface could be formed by a superposition of forcing by a negative wind stress curl (Ekman suction) and a poleward propagating Kelvin wave starting at the coast from the sea level plateau north of 14°S. The geostrophic currents adjusted to the observed dynamic topopgraphy consists of a remarkable jet like current in the upper 400 m entering the studied area from its north-western corner with a southward transport of about 6 Sv, bending southward at the shelf near 15°S and leaving the area of investigation with 7 Sv toward south. This current can be seen in the direct ADCP measurements as well as in the geostrophic analysis. The geostrophic transport balance of the area of investigation is closed by a week southward transport of about 1 Sv through its northern boundary. Evidence for a superposition of geostrophic current and Ekman offshore current in the surface mixed layer was found at both the southern cross section and the longitudinal section OS1 at the western rim of the studied area. On this sections the southerly wind was most pronounced. The offshore transport through the 300-km long section OS1 summed up to about 1 Sv.

In contrast to the hydrographic features the current field observed in the Angola–Benguela front area during the cruise differed considerable from the current pattern observed during the R/V *F. Nansen* cruise three weeks before (Boyd et al. 1998). This suggests that the current pattern measured during the cruise was a transient one. The pattern of the wind stress curl was quite different during the R/V *F. Nansen* cruise as well by the absence of the seaward extension of the coastal belt of negative wind stress curl.

The geostrophic circulation presented here seems to be a link between the cyclonic gyre in the tropical southeast Atlantic described by Moroshkin et al. (1970) and Gordon and Bosley (1991) and the circulation in the source region of the Benguela Current summarized by Peterson and Stramma (1991) and illustrated by Garzoli and Gordon (1996) and Garzoli et al. (1997) by time series measurements with inverted echo sounder and satellite altimeter, respectively. Controlled by the actual pattern of the wind stress curl distribution tropical water from the cyclonic gyre in the area of the Angola Dome may leak southward through the Angola–Benguela front as a poleward current along the continental shelf advecting tropical Atlantic thermocline water of low oxygen content southward. This poleward current may be transformed in an undercurrent in the area of the Benguela upwelling zone. Boyd et al. (1998) observed such undercurrent on the shelf just south of the Angola–Benguela front, Hagen (1991) found it at 22°S, and Gordon et al. (1995) measured it at 27°S, respectively. Shannon and Nelson (1996) summarized the current observations on the shelf of South West Africa between 22° and 34.5°S as an equatorward current in the surface layer and a poleward motion of varying strength between 40- and 600-m depth. The tropical water of this coastal current leaves the shelf region between 30° to 35°S toward the open ocean and contributes to the 3–4-Sv mean volume flux, which enters the source region of the Benguela Current from the east according to Garzoli and Gordon (1996) and Garzoli et al. (1997). This offshore volume

flux reveals significant temporal variability and is maximum during austral summer (4 Sv) and fall (5 Sv), which is in agreement with the observations of the coastal current described in this paper.

Several question could not be answered by the data acquired during the R/V *P. Kottzov* cruise. It is important to know how often and where the extension of the cyclonic wind stress curl into the open ocean does develop and whether it is related to the Angola Dome. The sections performed during the cruise were not extended far enough into the ocean to see how the circulation behaves on the seaward edge of the cyclonic gyre and whether there exists a closed link between the shelf edge current, the Benguela Current, the South Equatorial Counter Current, and the Angola Current.

Acknowledgments. The experimental phase of the studies was supported by the German Federal Ministry for Science and Technology which provided the Centre for Marine Tropical Ecology (ZMT) with the means to charter the vessel for the expedition. The assistance of the captain and his officers and crew of R/V *P. Kottzov* during the cruise is well recognized.

The field work and contributions of the following are acknowledged. Ashley Johnson, Sea Fisheries Research Institute in Cape Town; Christo Whittle, University of Cape Town; Chris Bartholomae, Aina Iita; Anja Risser, National Marine Information and Research Centre in Swakopmund; and Quilinda Fidel and Bomba Bazik Sangolay, Institute de Investigacao Pesqueira in Luanda.

Siegfried Krüger implemented the CTD systems on R/V *P. Kottzov* for both profiling and towing and kept them running during the cruise. Dietmar Ruess worked laboriously on implementation, calibration, programming, and performing the validation of the towed ADCP measurements. Toralf Heene carried the major load of the CTD data visualization. Birgit Sadkowiak processed the oxygen content of water samples.

Satellite images of SST were kindly provided in an online mode by Scarla Weeks of University of Cape Town. Chris Finch of JPL generously provided the NSCAT data in ASCII format.

We are grateful for the comments and suggestions of V. Shannon and an anonymous referee. V. Mohrholz was supported by the Deutsche Forschungsgemeinschaft (DFG), Grant Nr. LA 1137 1-1.

REFERENCES

Bakun, A., and C. S. Nelson, 1991: The seasonal cycle of wind-stress curl in subtropical eastern boundary current regions. *J. Phys. Oceanogr.,* **21,** 1815–1834.

Boebel, O., C. Schmid, and W. Zenk, 1997: Flow and recirculation of Antarctic Intermediate Water across the Rio Grande Rise. *J. Geophys. Res.,* **102** (C9), 20 967–20 986.

Boyd, A. J., 1987: The oceanography of the Namibian shelf. Ph.D. thesis, University of Cape Town, 190 pp. [Available from Department of Oceanography, University of Cape Town, Private Bag Rondebosch 7701, Republic of South Africa.]

——, C. H. Bartholomae, J. J. Agenbag, and T. Gammelsrod, 1998: The variability of near-surface currents in the Northern and Central Benguela. *Proc. Int. Symp. and Workshop on Environmental Variability in the South Atlantic,* Swakopmund, Namibia, Benguela Environment Fisheries Interaction and Training.

Bubnov, V. A., 1972: Structure and characteristics of the oxygen minimum layer in the southeastern Atlantic. *Oceanology,* **12,** 193–201.

Chapmann, P., and L. V. Shannon, 1985: The Benguela ecosystem. Part II. Chemistry and related processes. *Oceanogr. Mar. Biol.,* **23,** 183–251.

——, and ——, 1987: Seasonality in the oxygen minimum layers at the extremities of the Benguela system. *S. Afr. J. Mar. Sci.,* **5,** 85–94.

Defant, A., 1961: *Physical Oceanography.* Vol. 1. Pergamon Press, 729 pp.

Dias, C. A., 1983a: Note on the evidence of a permanent southward flow of the upper oceanic tropospheric waters off Angola at 12°S. *Collect. Sci. Pap. Int. Comm. Southeast. Atl. Fish.,* **10,** 99–102.

——, 1983b: Preliminary report on the physical oceanography off southern Angola, March and July 1971. *Collect. Sci. Pap. Int. Comm. Southeast. Atl. Fish.,* **10,** 103–116.

Duncombe Rae, C. M., 1998: Antarctic Intermedita and Central Waters in the Angola–Benguela front region: Results from the first BENEFIT cruise, April 1997. *Proc. Int. Symp. on Environmental Variabilty in the SE Atlantic,* Swakopmund, Namibia, Benguela Environment Fisheries Interaction and Training.

Fennel, W., 1999: Theory of the Benguela upwelling system. *J. Phys. Oceanogr.,* **29,** 177–190.

——, and H. U. Lass, 1989: *Analytical Theory of Forced Oceanic Waves.* Akademie-Verlag, 312 pp.

Gammelsrod, T., and Coauthors, 1997: Survey of the Angola Benguela front and the Angola Dome. Benefit Surveys Cruise Rep. 1/97, Institute of Marine Research, Bergen, Norway, 100 pp. [Available from Institute of Marine Research, P. B. 1870 Nordnes, 5817 Bergen, Norway.]

——, C. H. Bartholomae, D. C. Boyer, V. L. L. Filipe, and M. J. O'Toole, 1998: Intrusion of warm surface layers along the Angolan–Namibian coast in February–March 1995: The 1995 Benguela Nino. *Proc. Int. Symp. and Workshop on Environmental Variability in the South Atlantic,* Swakopmund, Namibia, Benguela Environment Fisheries Interaction and Training.

Garzoli, S. L., and A. L. Gordon, 1996: Origins and variability of the Benguela Current. *J. Geophys. Res.,* **101** (C1), 897–906.

——, G. J. Goni, A. J. Mariano, and D. B. Olson, 1997: Monitoring the upper southeastern transports using altimeter data. *J. Mar. Res.,* **55,** 453–481.

Gordon, A. L., and K. T. Bosley, 1991: Cyclonic gyre in the tropical South Atlantic. *Deep-Sea Res.,* **38,** 323–343.

Gordon, A. L., K. T. Bosley, and F. Aikman III, 1995: Tropical Atlantic water within the Benguela upwelling system at 27° S. *Deep-Sea Res.,* **42,** 1–12.

Grasshoff, K. 1983: Determination of oxygen. *Methods of Seawater Analysis,* K. Grasshoff, M. Ehrhardt, and K. Kremling, Eds., Verlag Chemie, 61–72.

Hagen, E., 1981: Mesoscale upwelling variations off the west African coast. *Coastal Upwelling,* F. A. Richards, Ed., Vol. 1, Coastal and Estuarine Sciences, Amer. Geophys. Union, 72–78.

——, 1991: Beobachtungen der täglichen und mehrtägigen Auftriebsvariabilität über dem Schelf von Namibia im Herbst 1976. *Beitr. Meereskd.,* **62,** 3–34.

Hellerman, S., and M. Rosenstein, 1983: Normal monthly wind stress over the world ocean with error estimates. *J. Phys. Oceanogr.,* **13,** 1093–1104.

Janke, J., 1920: Strömungen und Oberflächentemperaturen im Golf von Guinea. *Arch. Dtsch. Seewarte,* **28,** 1–68.

Joyce, T. M., 1989: On in situ ''calibration'' of shipboard ADCPs. *J. Atmos. Oceanic. Technol.,* **6,** 169–172.

Kostianoy, A. G., 1997: Application of satellite data to the analysis of fronts in the South-East Atlantic (Based on the example of

the Angola–Benguela Frontal Zone). *Earth Obs. Remote Sens.*, **14,** 613–626.

Lutjeharms, J. R. E., and J. M. Meeuwis, 1987: The extent and variability of Southeast Atlantic upwelling. *S. Afr. J. Mar. Sci.*, **5,** 51–62.

Mazeika, P. A., 1967: Thermal domes in the eastern Atlantic Ocean. *Limnol. Oceanogr.*, **12,** 537–539.

McClain, C. R., and J. Firestone, 1993: An investigation of Ekman upwelling in the North Atlantic. *J. Geophys. Res.*, **98** (C7), 12 327–12 339.

Meeuwis, J. M., and J. R. E. Lutjeharms, 1990: Surface thermal characteristics of the Angola–Benguela front. *S. Afr. J. Mar. Sci.*, **9,** 261–279.

Moroshkin, K. V., V. A. Bubnov, and R. P. Bulatov, 1970: Water circulation in the eastern South Atlantic Ocean. *Oceanology*, **10,** 27–34.

Nelson, G., and L. Hutchings, 1983: The Benguela upwelling area. *Progress in Oceanography*, Vol. 12, Pergamon, 333–356.

Petersen, R. G., and L. Stramma, 1991: Upper-level circulation in the South Atlantic Ocean. *Progress in Oceanography*, Vol. 26, Pergamon, 1–73.

Shannon, L. V., 1985: The Benguela ecosystem. Part I. Evolution of the Benguela, physical features and processes. *Oceanogr. Mar. Biol.*, **23,** 105–182.

——, and D. Hunter, 1988: Notes on Antarctic Intermediate Water around southern Africa. *S. Afr. J. Mar. Sci.*, **6,** 107–117.

——, and G. Nelson, 1996: The Benguela: Large scale features and processes and system variability. *The South Atlantic: Present and Past Circulation*, G. Wefer et al., Eds., Springer-Verlag, 163–210.

——, A. J. Boyd, G. B. Brundrit, and J. Taunton-Clark, 1986: On the existence of an El Nino-type phenomenon in the Benguela system. *J. Mar. Res.*, **44,** 495–520.

——, J. J. Agenbag, and M. E. L. Buys, 1987: Large and mesoscale features of the Angola–Benguela front. *S. Afr. J. Mar. Sci.*, **5,** 11–34.

Smith, D. S., 1988: Coefficients for sea surface wind stress, heat flux, and wind profiles as a function of wind speed and temperature. *J. Geophys. Res.*, **93** (C12), 15 467–15 472.

van Aken, H. M., 1986: The onset of stratification in shelf seas due to differential advection in the presence of a salinity gradient. *Contin. Shelf Res.*, **5,** 475–485.

Wacongne, S., and B. Piton, 1992: The near-surface circulation in the northeastern corner of the South Atlantic Ocean. *Deep-Sea Res.*, **39,** 1273–1298.

Yamagata, I., and S. Iizuka, 1995: Simulation of the tropical thermal domes in the Atlantic: A seasonal cycle. *J. Phys. Oceanogr.*, **25,** 2129–2140.